数理解析研究所講究録
第800巻 1992年 207-216

Sublayer Streaksの発生機構に関する一考察

愛媛大 工　河原 源太 (Genta Kawahara)

I. INTRODUCTION

One of the most outstanding characteristics of near-wall turbulence is the presence of streaky structures which consist of regions of low- and high-speed fluid, elongated downstream and alternating in the spanwise direction.[1] As is well known, these structures have a characteristic spanwise wavelength of approximately 100 wall units in the near-wall region, and their wavelength increases as the distance from the wall is increased.[2,3] They are believed to be a significant factor in the production and maintenance of a mean turbulent flow, since these structures were found to undergo so-called "bursting".[1,4] In a recent study,[5] the streaky structures were found to be associated with the vortical structures, i.e., the quasi-streamwise vortices, which play a dominant role in turbulence production and momentum transfer in the near-wall region, but their cause has been unclear.

Several attempts[6-8] have been made to give a theoretical explanation for the generation of the streaky structures. They succeeded in estimating the wavelengths corresponding to the mean streak spacing, but their results have not included the variation of the spacing with the distance from the wall. Recently, Lee *et al.*[9] studied a homogeneous shear flow at a high shear rate using the direct numerical simulation and rapid distortion theory (RDT). They showed that the presence of the wall is not necessary for the generation of the streaky structures, and that the essential mechanism responsible for the formation of these structures is contained in the *linear* theory. Lee and Hunt[10] studied an inhomogeneous uniform-shear flow with the slip condition at the plane boundary using RDT, and found that the streak spacing increases with the distance from the wall. However, it may be difficult to compare directly the streaky structures which Lee *et al.* and Lee and Hunt found with those in near-wall turbulent flows, since their results seem to depend on the initial conditions and a uniform mean shear was assumed.

In their computation based on the localized-induction approximation (LIA), Aref and Flinchem[11] found that localized finite-amplitude initial disturbances disperse into planar undulations on the vortex filament in the background shear. Since these undulations have

a certain well-defined periodicity and can lead to the generation of streamwise vorticity, such vortex dynamics is conjectured to be connected with the formation of the streaky structures. Pierrehumbert[12] pointed out that the vortex filament considered in Aref and Flinchem is unstable to infinitesimal disturbances, and showed that the linear stability theory can predict the wavelength of these undulations. However, there are some problems in the LIA, as is referred to by both authors. There is no objective way of evaluating the *constant* C, and C in reality depends logarithmically on wavenumber,[13] where C is the asymptotic expansion parameter coming from the LIA in Refs. 11 and 12. Moreover, it is difficult to examine the wall effect.

In this paper, a new phenomenological approach to the early stages of the formation of the streaky structures is described, which is based on the linear stability theory for a rectilinear vortex in a background shear flow. The Biot-Savart integral is carried out to study the long-wavelength instability. The cutoff method, proposed by Crow[14] and Moore and Saffman[15] is used to omit the singularity from the line integral. In this method, a cutoff length is evaluated with a vortex core radius. The core radius and the strength of the disturbed vortices are estimated from Robinson's[16] results for the transverse vortices in the numerically-simulated turbulent boundary layer. The most unstable spanwise wavelengths are calculated for the turbulent boundary-layer type background flow to be compared with the mean streak spacing. In addition, image vortices are introduced into the calculations to examine the effect of the wall impermeability.

II. INSTABILITY OF A VORTEX FILAMENT IN A SHEAR FLOW

The problem considered is a vortex filament embedded in a shear flow, as shown in Fig. 1. $\boldsymbol{e}_x$, $\boldsymbol{e}_y$ and $\boldsymbol{e}_z$ are the longitudinal, vertical and lateral unit vectors, and x, y and z are used to represent the coordinates corresponding to their directions. a is the vortex core radius, and Γ is the strength of the vortex filament. $\boldsymbol{U}_{ext} = U(y)\boldsymbol{e}_x$ is the background velocity field. In the absence of perturbations, the vortex is parallel to the z-direction.

The instantaneous flow due to the vortex filament is described by the Biot-Savart law with a cutoff, viz.:

$$\boldsymbol{u}(\boldsymbol{x},t) = -\frac{\Gamma}{4\pi}\int_{L[\delta]} \frac{\boldsymbol{x}-\boldsymbol{x}'}{|\boldsymbol{x}-\boldsymbol{x}'|^3}\times d\boldsymbol{x}' + \boldsymbol{U}_{ext}(\boldsymbol{x}). \tag{1}$$

Here $\boldsymbol{x} = x\boldsymbol{e}_x + y\boldsymbol{e}_y + z\boldsymbol{e}_z$, and the notation $\int_{L[\delta]}$ means that a length 2δ centered on $\boldsymbol{x}' = \boldsymbol{x}$ is omitted from a line integral along L defining the vortex. Given the fluid velocity $\boldsymbol{u}$, the equation of motion of the vortex for each point $\boldsymbol{X} = X\boldsymbol{e}_x + Y\boldsymbol{e}_y + Z\boldsymbol{e}_z$ on the filament is of the form

$$\frac{d\boldsymbol{X}(\boldsymbol{X}_0, t)}{dt} = \boldsymbol{u}(\boldsymbol{X}(\boldsymbol{X}_0, t), t), \tag{2}$$

where

$$\boldsymbol{X}(\boldsymbol{X}_0, t)|_{t=0} = \boldsymbol{X}_0. \tag{3}$$

The equation of motion is valid in the limit of small vortex cross-sectional area and long disturbance wavelength. In addition, it is valid only at early times in the evolution of the vortex. Consider the rectilinear vortex filament perturbed by a sinusoidal disturbance:

$$\begin{pmatrix} X \\ Y \\ Z \end{pmatrix} = \begin{pmatrix} U(y_0)t \\ y_0 \\ z \end{pmatrix} + \begin{pmatrix} \tilde{x} \\ \tilde{y} \\ 0 \end{pmatrix} \exp(i(kz - \sigma t)). \tag{4}$$

Here k is the axial wavenumber, σ is the growth rate, and y_0 is the y-location of the undisturbed vortex. Substituting into equation (2) and linearizing, we obtain

$$\left.\begin{aligned} -i\sigma\tilde{x} &= \frac{\Gamma}{2\pi}\omega(k\delta)k^2\tilde{y} + U'\tilde{y}, \\ -i\sigma\tilde{y} &= -\frac{\Gamma}{2\pi}\omega(k\delta)k^2\tilde{x}, \end{aligned}\right\} \tag{5a,b}$$

where

$$U' = \left.\frac{dU}{dy}\right|_{y=y_0}, \tag{6}$$

$$\omega(\xi) = \frac{1}{2}\left(\frac{\cos\xi - 1}{\xi^2} + \frac{\sin\xi}{\xi} - Ci(\xi)\right). \tag{7}$$

The function ω is Crow's self-induction function. Ci is the integral cosine function. A long-wavelength asymptote of ω is of the form

$$\omega \sim \frac{1}{2}\left(\ln\frac{1}{k\delta} - \gamma + \frac{1}{2}\right), \tag{8}$$

where $\gamma = 0.5772\cdots$ is Euler's constant, and the leading-order term depends logarithmically on wavenumber. The physical meanings of each term in equations (5) are similar to those of Pierrehumbert[12]. The first terms in (5) yield the self-induced rotation, and the second term in (5a) comes from the advection by the background shear flow. However, in the present

case the self-induced rotation rate is $O(-k^2 \ln k)$ for the long-wavelength disturbances, while in the LIA that is $O(k^2)$.

Moore and Saffman[15] assumed that the cutoff length δ depends only on the distribution of swirl and axial velocity in the vortex core, and found the value of δ by evaluating the Biot-Savart integral similar to (1) for a circular vortex ring and comparing with Saffman's[17] result for its translational velocity. The cutoff method has been applied to several stability problems, and it has been shown that it is useful to analyse the long-wavelength instabilities of rectilinear vortices.[14,18,19] When we assume uniform vorticity and no axial velocity in the core, δ is estimated from their formula

$$\delta = \tfrac{1}{2} e^{\frac{1}{4}} a. \tag{9}$$

Note that the asymptotic theory using the cutoff method is accurate to $O(ka)^2$. The dimensionless eigenvalues and corresponding eigenvectors of (5) are given by

$$\frac{\pi a^2 \sigma}{|\Gamma|} = \pm \frac{1}{2} \sqrt{\phi(ka)(\phi(ka) - 2\beta)}, \tag{10}$$

$$\frac{\tilde{y}}{\tilde{x}} = \mp \frac{i \frac{\Gamma}{|\Gamma|} \phi(ka)}{\sqrt{\phi(ka)\,(\phi(ka) - 2\beta)}}, \tag{11}$$

where

$$\phi(\xi) = \xi^2 \omega(\tfrac{1}{2} e^{\frac{1}{4}} \xi), \tag{12}$$

$$\beta = -\frac{\pi a^2 U'}{\Gamma}. \tag{13}$$

β indicates the ratio of circulation of the background shear to that of the vortex. The stability of the vortex filament depends only on β, and the vortex can be unstable when it has circulation of the same sign as that of the background shear ($\beta > 0$). The physical mechanism of the instability is qualitatively the same as that discussed by Pierrehumbert.[12] When $\beta > 0$, the self-induced rotation is opposite to the background rotation and the background strain dominates the stabilizing effect of the self-induced rotation, depressed by the background rotation. The unstable band of ϕ is $0 < \phi < 2\beta$, and the unstable modes lie in a plane tilted to the (x, z)-plane, which lead to the generation of streamwise vorticity. The maximum growth occurs at

$$\phi(ka) = \beta, \tag{14}$$

and in this case the eigenvector is tilted at a 45° angle to the (x, z)-plane.

Figure 2 is the resulting stability diagram. It is found that as β increases, the vortex becomes unstable to the larger-wavenumber disturbances and the most unstable mode has the larger wavenumber. Note that a short-wavelength instability ($ka \approx 1$), allowed by the cutoff theory is valid only in a qualitative sense.

III. THE MOST UNSTABLE WAVELENGTH FOR THE TRANSVERSE VORTICES IN THE TURBULENT BOUNDARY-LAYER TYPE BACKGROUND FLOW

The vortex instability discussed in Sec. II is considered for the background or mean flow with the same velocity profile as that of turbulent channel flow.[3] Robinson[16] identified the elongated low-pressure regions corresponding to the vortical structures in Spalart's[20] numerically-simulated boundary layer, and showed the kinematic properties of transverse vortices in the near-wall region. In the present study, the core radius and the strength of the disturbed vortices are estimated from Robinson's[16] results for the transverse vortices, viz.:

$$a^+ = \tfrac{1}{2}\kappa y^+, \tag{15}$$

$$\Gamma^+ = 2\pi R_V. \tag{16}$$

Here $\kappa = 0.41$ is the Karman constant, and y is the vortex core height. Hereinafter the notaion $^+$ indicates a value normalized by wall variables, i.e., ν and u_τ, where ν is kinematic viscosity and u_τ is a friction velocity. $R_V = \Gamma/2\pi\nu \approx -30$ is the most probable value of a vortex Reynolds number for the transverse vortices, computed with the fluctuating component of spanwise vorticity. He reported that the variation of the transverse-vortex radius with the distance from the wall is fit reasonably well by equation (15), and that over 40% of the transverse vortices is distributed over the vicinity of R_V. Although the vortical structures including the transverse-vortex parts, identified by Robinson seem to have already evolved into a three-dimensional shape, in the present study we examine the instability of the rectilinear vortex with the same radius and strength as those of the transverse vortex. We are also interested in the *long-wavelength* instability, since the

lengthscale of the above transverse-vortex radius is much smaller than that of the streak spacing (≈ 100 in wall units) in the near-wall region.

The above instability parameter β is plotted as a function of y^+ in Fig. 3. The vortex can be unstable for such a value of β, as discussed in Sec. II. As y^+ is increased, β increases monotonically. However, β is of the order of 10^{-1} in the near-wall region, which means that the magnitude of vorticity of the vortex is much larger than that of vorticity and strain of the background or mean shear. For such weak strain, the growth rate predicted by the Biot-Savart cutoff theory is in excellent agreement with an exact one at small wavenumber.[19]

The growth rate Im σ^+ is shown in Fig. 4. The maximum growth rate decreases and the most unstable dimensionless wavenumber ka increases with y^+. In addition, the dimensionless-wavenumber range, in which the instability occurs, grows broader as y^+ is increased, i.e., β is increased, which means that the vortex can be unstable to the disturbances with the wavelength comparable to the vortex radius. The maximum growth, however, occurs at $ka < 0.5$, when the vortex is located at $y^+ \leq 70$.

The variation of the most unstable wavelength λ^+ with the distance from the wall is shown in Fig. 5. Figure 5 includes the results for the viscous sublayer ($0 < y^+ < 5$) to show the effect of image vortices, but it is doubtful whether the invisid theory can be applied to this region. The vortex radius a increases with y^+, which increases λ^+ for fixed β. On the other hand, the instability parameter β increases with y^+, which decreases λ^+ for fixed a as shown in Fig. 4. The variation of λ^+ is determined by the above both effects. The resulting dependence of λ^+ on the distance from the wall is found to be similar to that of the recent experimental results[21] for the mean streak spacing near the wall. Moreover, it is found that the most unstable mode has a spanwise wavelength of about 100 wall units in the buffer region ($5 < y^+ < 30$). We also consider the effect of image vortices, introduced into the calculations (see Appendix). With an image vortex, λ^+ approaches zero linearly as $y^+ \to 0$, while without an image vortex, it approaches infinity. At $y^+ > 10$, both wavelengths are similar and image vortices only decrease the wavelength slightly. The effect of image vortices on the shear instability is found to be limited only to the vicinity of the wall ($y^+ < 10$), which suggests that the wall impermeability may not be necessary for the generation of the streaky structures, as is pointed out by Lee *et al.*[9]

The present results are compared with representative experimental results for the mean

streak spacing taken from Kasagi,[22] as shown in Fig. 6. At $10 < y^+ < 60$, they have the same trend as that of the present results, although there are some deviations in the experimental results. It suggests that the vortex instability discussed in Sec. II may show the early stages of the formation of the streaky structures, and that their spanwise dimensions may be fixed in these stages. At $y^+ > 60$, it is difficult to compare the present results with the experimental results, since there are few data, distributed over the wide range in this region. We conjecture that the variation of the streak spacing with the distance from the wall may be determined rather by the dynamical behavior of the streaks, e.g., the spacing is increased as the streaks generated near the wall ascend from there, than by the above vortex instability. However, it is beyond the present study to discuss how the transverse vortices are generated, how their cross-sectional lengthscale and circulation are determined, and the effect of the internal structure of the transverse vortices.

APPENDIX: INTRODUCTION OF IMAGE VORTICES

When image vortices are introduced, equations (5) are rewritten in the form

$$\left.\begin{aligned} -i\sigma\tilde{x} &= -\frac{\Gamma}{2\pi b^2}\tilde{y} - \frac{\Gamma}{2\pi b^2}\chi(kb)\tilde{y} + \frac{\Gamma}{2\pi}\omega(k\delta)k^2\tilde{y} + U'\tilde{y}, \\ -i\sigma\tilde{y} &= -\frac{\Gamma}{2\pi b^2}\tilde{x} + \frac{\Gamma}{2\pi b^2}\psi(kb)\tilde{x} - \frac{\Gamma}{2\pi}\omega(k\delta)k^2\tilde{x}, \end{aligned}\right\} \qquad (A1a,b)$$

where b is the distance between the real and image vortices,

$$\chi(\xi) = \xi K_1(\xi), \qquad (A2)$$

$$\psi(\xi) = \xi^2 K_0(\xi) + \xi K_1(\xi). \qquad (A3)$$

The functions χ and ψ are Crow's first and second mutual-induction functions. K_0 and K_1 are modified Bessel functions of the second kind. The dimensionless eigenvalues and corresponding eigenvectors of (A1) are given by

$$\frac{\pi a^2\sigma}{|\Gamma|} = \pm\frac{1}{2}\sqrt{(\phi(ka) - \alpha^2\psi(\alpha^{-1}ka) + \alpha^2)(\phi(ka) - 2\beta - \alpha^2\chi(\alpha^{-1}ka) - \alpha^2)}, \qquad (A4)$$

$$\frac{\tilde{y}}{\tilde{x}} = \mp\frac{i\frac{\Gamma}{|\Gamma|}(\phi(ka) - \alpha^2\psi(\alpha^{-1}ka) + \alpha^2)}{\sqrt{(\phi(ka) - \alpha^2\psi(\alpha^{-1}ka) + \alpha^2)(\phi(ka) - 2\beta - \alpha^2\chi(\alpha^{-1}ka) - \alpha^2)}}, \qquad (A5)$$

where $\alpha = a/b$, and it has a constant value of $\kappa/4$ in the present case. Without a background shear, the above formulae were given by Crow [14].

REFERENCES

[1]S. J. Kline, W. C. Reynolds, F. A. Schraub and P. W. Runstadler, J. Fluid Mech. **30**, 741 (1967).

[2]C. R. Smith and S. P. Metzler, J. Fluid Mech. **129**, 27 (1983).

[3]J. Kim, P. Moin and R. D. Moser, J. Fluid Mech. **177**, 133 (1987).

[4]H. T. Kim, S. J. Kline and W. C. Reynolds, J. Fluid Mech. **50**, 133 (1971).

[5]S. K. Robinson, S. J. Kline and P. R. Spalart, in *Near-Wall Turbulence: 1988 Zoran Zaric Memorial Conference*, edited by S. J. Kline and N. H. Afgan (Hemisphere, New York, 1990), p. 218.

[6]F. H. Bark, J. Fluid Mech. **70**, 229 (1975).

[7]Z. Zhang and G. M. Lilley, in *Third Symposium on Turbulent Shear Flows, Davis, California, September 9-11, 1981*, edited by L. J. S. Bradbury *et al.*, p. 11.24.

[8]P. S. Jang, D. J. Benney and R. L. Gran, J. Fluid Mech. **169**, 109 (1986).

[9]M. J. Lee, J. Kim and P. Moin, in *Sixth Symposium on Turbulent Shear Flows, Toulouse, France, September 7-9, 1987*, edited by F. Durst *et al.*, p. 22.6.1.

[10]M. J. Lee and J. C. R. Hunt, in *Seventh Symposium on Turbulent Shear Flows, Stanford University, Stanford, California, August 21-23, 1989*, edited by F. Durst *et al.*, p. 8.1.1.

[11]H. Aref and E. P. Flinchem, J. Fluid Mech. **148**, 477 (1984).

[12]R. T. Pierrehumbert, J. Fluid Mech. **163**, 21 (1986).

[13]D. W. Moore and P. G. Saffman, in *Aircraft Wake Turbulence and Its Detection*, edited by J. H. Olsen *et al.* (Plenum Press, New York, 1971), p. 339.

[14]S. C. Crow, AIAA J. **8**, 2172 (1970).

[15]D. W. Moore and P. G. Saffman, Phil. Trans. R. Soc. Lond. A **272**, 403 (1972).

[16]S. K. Robinson, in *Structure of Turbulence and Drag Reduction: IUTAM Symposium Zurich, Switzerland, July 25-28, 1989*, edited by A. Gyr (Springer-Verlag, Berlin, 1990), p. 23.

[17]P. G. Saffman, Stud. Appl. Math. **49**, 371 (1970).

[18]S. E. Widnall, Ann. Rev. Fluid Mech. **7**, 141 (1975).

[19]A. C. Robinson and P. G. Saffman, J. Fluid Mech. **142**, 451 (1984).

[20]P. R. Spalart, J. Fluid Mech. **187**, 61 (1988).

[21]Y. Iritani, N. Kasagi and M. Hirata, Trans. JSME B **51**, 3092 (1985).

[22]N. Kasagi, in *Near-Wall Turbulence: 1988 Zoran Zaric Memorial Conference*, edited by S. J. Kline and N. H. Afgan (Hemisphere, New York, 1990), p. 596.

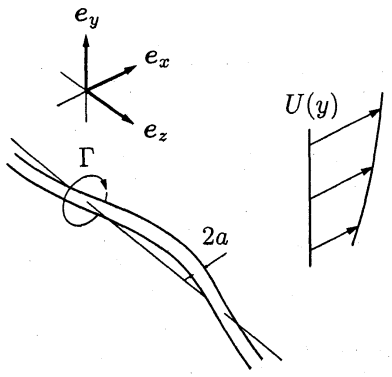

Fig. 1. Definition of problem showing the unit vectors corresponding to the coordinates. In this case, the vortex has circulation of the same sign as that of the background shear.

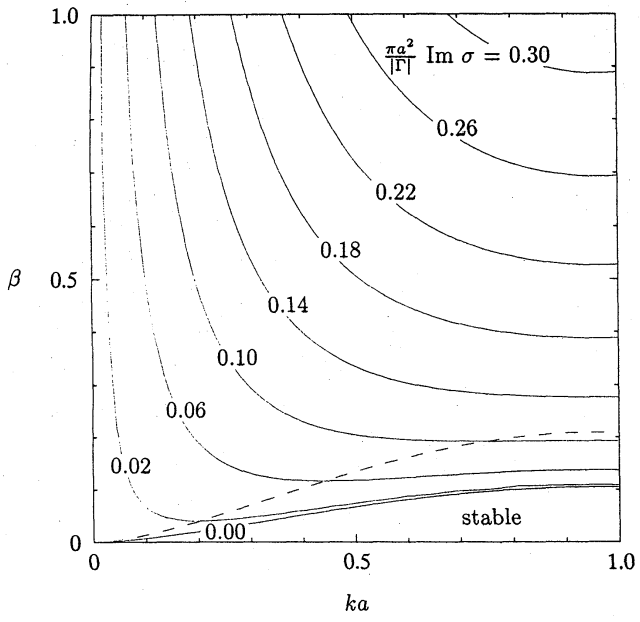

Fig. 2. Contour plot of growth rate in ka and β. The dashed line indicates ka at which maximum growth occurs for fixed β.

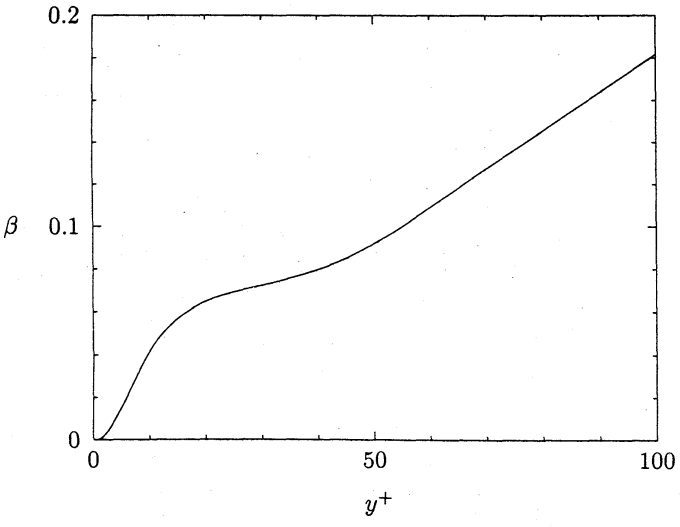

Fig. 3. Plot of instability parameter β versus y^+.

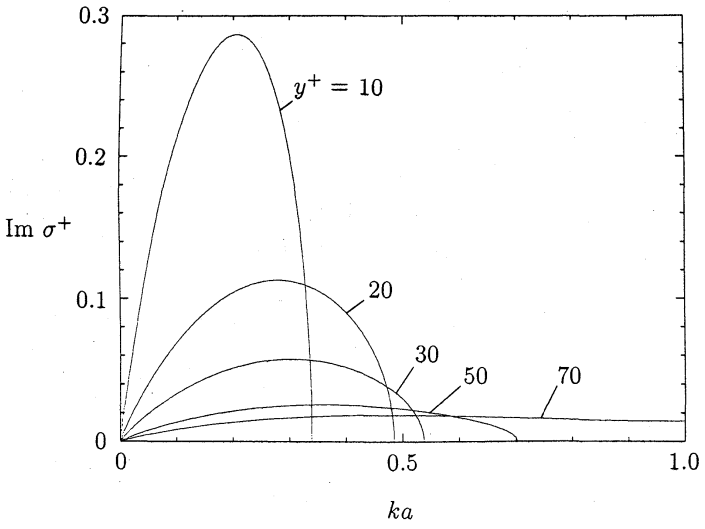

Fig. 4. Growth rate versus ka for various y^+-locations.

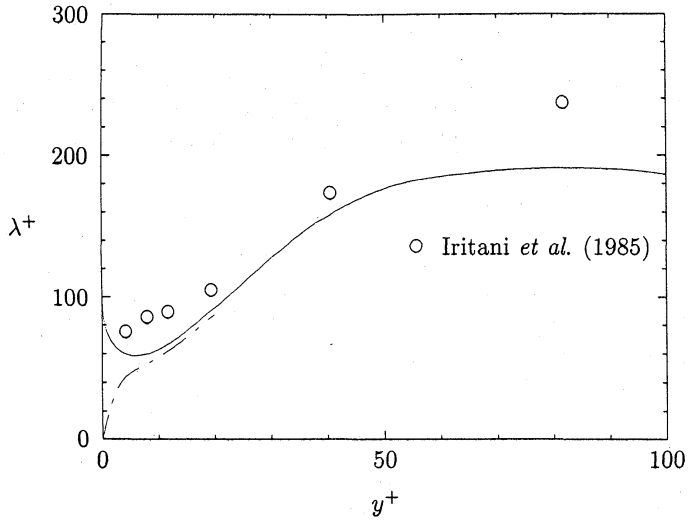

Fig. 5. Dependence of the most unstable spanwise wavelength on y^+. The solid line indicates the results without an image vortex. The dotted-dashed line indicates the results with an image vortex.

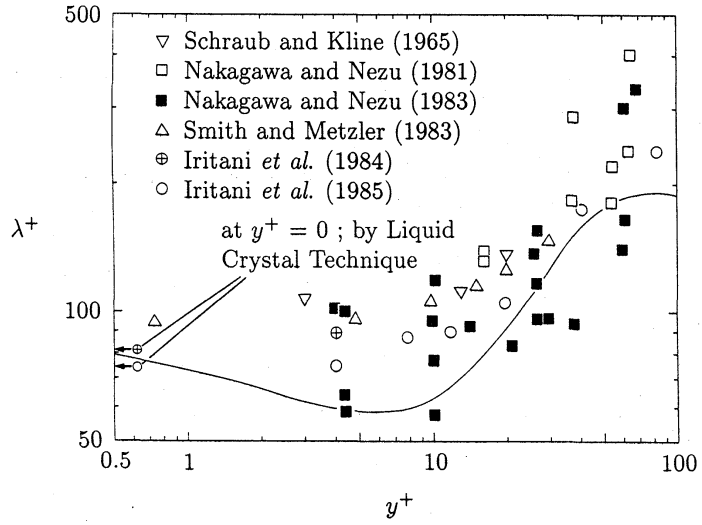

Fig. 6. Comparison of the most unstable spanwise wavelength with representative experimental results for the mean streak spacing taken from Kasagi[22].